arXiv:1602.05849v3 [hep-ph] 18 Mar 2016

Self Coupling of the Higgs boson in the processes $p\,p \to ZHHH + X$ and $p\,p \to WHHH + X$

Duane A. Dicus,[1,*] Chung Kao,[2,†] and Wayne W. Repko[3,‡]

[1] *Department of Physics, University of Texas, Austin, TX 78712, USA*

[2] *Homer L. Dodge Department of Physics, University of Oklahoma, Norman, OK 73019, USA*

[3] *Department of Physics and Astronomy, Michigan State University, East Lansing, MI 48824, USA*

(Dated: March 21, 2016)

To gain some sense about the likelihood of measuring the Higgs boson quartic coupling, we calculate the contribution to the triple Higgs production cross section from the subprocesses $q\bar{q} \to ZHHH$ and $q\bar{q}' \to WHHH$. Our results illustrate that determining this coupling, or even providing experimental evidence that it exists, will be very difficult.

PACS numbers: 13.38.Dg

* dicus@physics.utexas.edu
† kao@physics.ou.edu
‡ repko@pa.msu.edu

I. INTRODUCTION

The Standard Model (SM) has been very successful in explaining almost all experimental data to date, culminating in the discovery of the long awaited Higgs boson at the CERN Large Hadron Collider (LHC) [1, 2]. The most important experimental goals of Run 2 at the Large Hadron Collider are the investigation of Higgs properties and the search for new physics beyond the Standard Model.

Thus far the results from the LHC indicate that the couplings of the Higgs boson to other particles are consistent with the Standard Model. However the ultimate test as to whether this particle is the SM Higgs boson will be the trilinear Higgs coupling that appears in Higgs pair production and the quartic Higgs coupling that shows up in triple Higgs production.

The self interaction of the Higgs field, H, is

$$V(H) \,=\, \lambda\, v^2\, H^2 \,+\, \kappa_3 \lambda\, v\, H^3 \,+\, \frac{1}{4}\kappa_4\, \lambda\, H^4 \tag{1}$$

where $\lambda\, v^2 \,=\, \frac{1}{2} m_H^2$ and v is the vacuum expectation value given by the Z mass, M_Z, the weak mixing angle θ_W, and the fine structure constant α as $v \,=\, M_Z\, \cos\theta_W \sin\theta_W/\sqrt{\pi\alpha}$. κ_3 and κ_4 are one in the standard model; these are what we would like to measure.

To get a feeling for the relative strengths of the terms in Eq. (1) above we consider here the contribution of the subprocesses $q\bar{q} \,\to\, ZHHH$ to $p\,p \,\to\, ZHHH + X$ and $q\bar{q} \,\to\, W^+HHH$ to $p\,p \,\to\, W^+HHH + X$. Typical diagrams for this process are shown in Fig. (1).

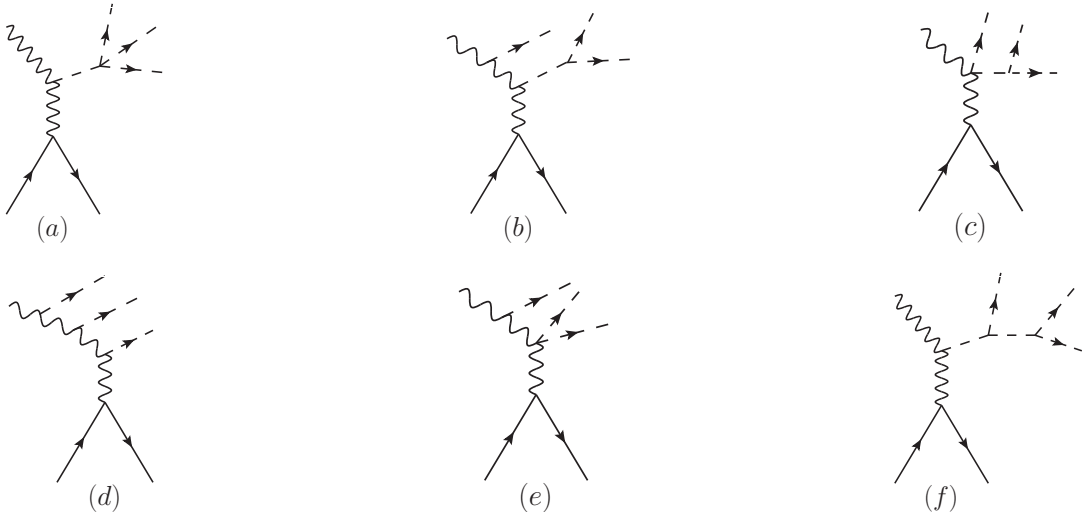

FIG. 1. Typical diagrams for the process $q\bar{q} \,\to\, ZHHH$ are shown. The same set applies to $q\bar{q} \,\to\, W^{\pm}HHH$.

II. CONTRIBUTIONS FROM TRILINEAR AND QUARTIC COUPLINGS

The matrix element from the Feynman diagrams above has terms of the form

$$\mathcal{M} \,\sim\, A\kappa_4 + B\kappa_3 + C + D\kappa_3^2\,, \tag{2}$$

where A comes from diagram (a), B from diagrams (b) and (c), C from diagrams (d) and (e), and D from diagram (f). The total cross section is given by

$$\sigma \,=\, \kappa_4^2\, \sigma_{44} \,+\, \kappa_3^2\, (\sigma_{33} + \sigma_{330}) \,+\, \sigma_0 \,+\, \kappa_4\kappa_3\sigma_{43} \,+\, \kappa_4\sigma_{40} \,+\, \kappa_3\sigma_{30} \,+\, \kappa_3^4\sigma_{3333} \,+\, \kappa_4\kappa_3^2\sigma_{433} \,+\, \kappa_3^3\sigma_{333}\,, \tag{3}$$

where

$$\begin{array}{llll} \sigma_{44} & \sim |A|^2 & \sigma_{33} & \sim |B|^2 \\ \sigma_{330} & \sim C\,D^* + C^*\,D & \sigma_0 & \sim |C|^2 \\ \sigma_{43} & \sim A\,B^* + A^*\,B & \sigma_{40} & \sim A\,C^* + A^*\,C \\ \sigma_{30} & \sim B\,C^* + B^*\,C & \sigma_{3333} & \sim |D|^2 \\ \sigma_{433} & \sim A\,D^* + A^*\,D & \sigma_{333} & \sim B\,D^* + B^*\,D \end{array} \tag{4}$$

These separate cross sections for the various terms in Eq. (3), in femtobarns, for several center of mass energies, are given in Table I for Z and Table II for W^+. These were derived using CTEQ6L1 distribution functions [3] with scale $\sqrt{\hat{s}}$. We do not include any contribution from gq or gg initial states. A K factor of [4]

$$K \;=\; 1 + \frac{\alpha_s}{2\pi}\pi^2\frac{16}{9} \;\approx\; 1.3 \tag{5}$$

was included where

$$\alpha_s^{-1} \;=\; \frac{1}{0.130} + \frac{21}{12\pi}\log(\frac{\hat{s}}{M_t^2}) + \frac{46}{12\pi}\log\frac{M_t}{M_Z}\,. \tag{6}$$

For the process $pp \;\to\; ZHHH + X$, the contents of Table I are illustrated in Fig. 2. The figure for $pp \;\to\; W^+HHH + X$ is similar.

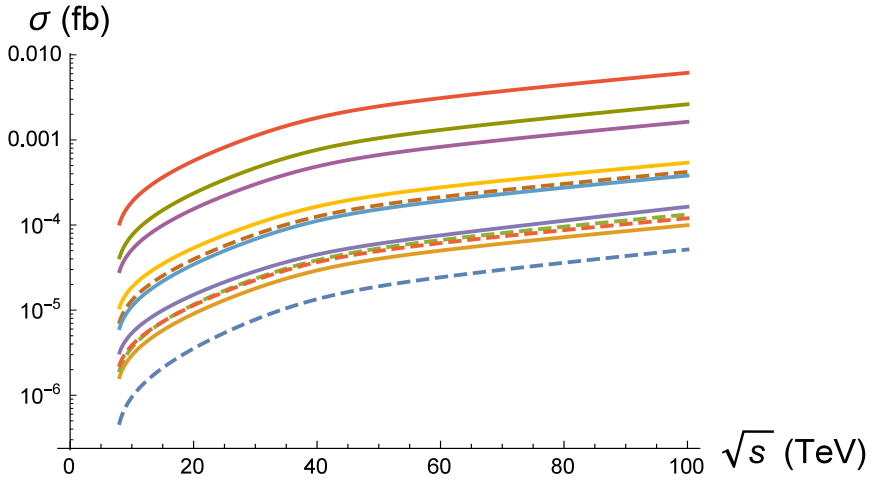

FIG. 2. The various contributions to the total cross section for $pp \;\to\; ZHHH + X$ are shown as a function of $\sqrt{s}$. The ordering of the curves corresponds to the ordering of the columns in Table I. σ_{44} is the lowest curve and σ_{TOT} is the highest. The contributions involving the quartic coupling are indicated by dashed lines.

The amplitude C in Eq. (2) comes from the ZZH and $ZZHH$ couplings (diagrams (d) and (e)). Superficially these diagrams grow faster with energy than the diagrams that involve Higgs propagators. However, the largest energy behavior cancels between the diagrams with only ZHH couplings and those that involve a ZZH and a $ZZHH$ coupling. Explicitly implementing this cancellation of the large energy behavior seems essential for the calculation of σ_0; depending on the phase space integral to find the cancellation does not work for large center of mass energies. A similar high energy behavior occurs in the W^+ cross section and requires the same analytic cancellation. A detailed description of how this cancellation occurs is given in the next section.

III. CANCELLATION OF THE LEADING HIGH ENERGY BEHAVIOR

If we label the momenta as

$$q(p_1) + \bar{q}(p_2) \;\to\; H(k_1) + H(k_2) + H(k_3) + Z(P) \tag{7}$$

then the matrix element for C can be written

$$M \sim \bar{v}(p_2)\gamma_\mu(g_V - \gamma_5)u(p_1)X^{\mu\lambda}\epsilon_\lambda(P) \tag{8}$$

The spinor factor goes as E^1 at large energy E. $X^{\mu\lambda}$ has two or three Z propagators depending on the diagram. The propagator which couples to the spinor factor goes as E^{-2} because the momentum in the $p^\mu p^\nu/M_Z^2$ term is $p_1 + p_2$ which is zero when dotted into spinor factor. The other one or two propagators do not have this cancellation and thus go as E^0. The Z polarization vector can be longitudinal and thus go as E^1. So these diagrams go as E^0 for large E. The diagrams for contributions other than C go as E^{-2} or faster because they have Higgs propagators.

To see this E^0 behavior cancel we need to write out $X^{\mu\lambda}$

$$\begin{aligned} X^{\mu\lambda} &= \frac{1}{2}A_1^{\mu\rho}(B_{2\rho}^\lambda + B_{3\rho}^\lambda + g_\rho^\lambda) + \frac{1}{2}A_2^{\mu\rho}(B_{1\rho}^\lambda + B_{3\rho}^\lambda + g_\rho^\lambda) + \frac{1}{2}A_3^{\mu\rho}(B_{1\rho}^\lambda + B_{2\rho}^\lambda + g_\rho^\lambda) \\ &+ \frac{1}{2}(A_1^{\mu\rho} + A_2^{\mu\rho} + g^{\mu\rho})B_{3\rho}^\lambda + \frac{1}{2}(A_2^{\mu\rho} + A_3^{\mu\rho} + g^{\mu\rho})B_{1\rho}^\lambda + \frac{1}{2}(A_1^{\mu\rho} + A_3^{\mu\rho} + g^{\mu\rho})B_{2\rho}^\lambda \end{aligned} \tag{9}$$

where

$$A_i^{\mu\lambda} = C_i(M_Z^2 g^{\mu\lambda} + k_i^\mu Q_i^\lambda) \quad \text{no sum on i} \tag{10}$$

$$B_i^{\mu\lambda} = D_i(M_Z^2 g^{\mu\lambda} - R_i^\mu k_i^\lambda) \quad \text{no sum on i} \tag{11}$$

for $i = 1, 2, 3$ with

$$Q_i^\mu = p_1^\mu + p_2^\mu - k_i^\mu \tag{12}$$

$$R_i^\mu = P^\mu + k_i^\mu \tag{13}$$

and

$$C_i = \frac{1}{Q_i^2 - M_Z^2} \tag{14}$$

$$D_i = \frac{1}{R_i^2 - M_Z^2} \tag{15}$$

The large E behavior comes from the $P^\mu P^\nu/M_Z^2$ part of the sum over Z polarizations, so replace the polarization vector $\epsilon_\lambda(P)$ by P_λ and dot P_λ into $X^{\mu\lambda}$. Then use

$$D_i^{-1} = 2P\cdot k_i + \frac{1}{2}m_H^2 \tag{16}$$

to eliminate $P\cdot k_i$ factors in favor of mass factors or the cancellation of D_i terms. The remaining large E terms will occur in the combination $C_i(p_1 + p_2 - k_i)^2$, which can be replaced by M_Z^2 and terms that vanish when contracted with the lepton factor. In particular if we define

$$F_i^\rho = D_i[M_Z^2 P^\rho + \frac{1}{2}M_H^2(P + k_i)^\rho] \tag{17}$$

then

$$\begin{aligned} X^{\mu\rho}P_\rho &= \frac{1}{2}A_i^{\mu\rho}(F_{j\rho} + F_{k\rho}) + \frac{1}{2}[A_i^{\mu\rho} + A_j^{\mu\rho} + g^{\mu\rho}]F_{k\rho} \\ &\equiv X^\mu \end{aligned} \tag{18}$$

where

$$i, j, k = (1, 2, 3) + (2, 3, 1) + (3, 1, 2) \tag{19}$$

and F_i^ρ is smaller than $B_i^{\rho\lambda}P_\lambda$ by two factors of mass rather than momenta. (The terms with the additional factors of momenta are proportional to $P^\mu + k_1^\mu + k_2^\mu + k_3^\mu = p_1^\mu + p_2^\mu$ dotted into the spinor factor.)

If we call the square of the spinor factor in Eq. (8), summed over spins, $L_{\mu\nu}$, then the square of the matrix element for σ_0, including the transverse polarizations of the Z, is

$$\sum_{pol} |M|^2 \sim L_{\mu\nu} X^{\mu\lambda} X^{\nu\eta} (-g_{\lambda\eta}) + L_{\mu\nu} X^\mu X^\nu / M_Z^2 \tag{20}$$

where X^μ, defined in Eq. (18) above, can be simplified to

$$X^\mu = A_1^{\mu\rho}(F_{2\rho} + F_{3\rho}) + A_2^{\mu\rho}(F_{1\rho} + F_{3\rho}) + A_3^{\mu\rho}(F_{1\rho} + F_{2\rho}) + \frac{1}{2} g^{\mu\rho}(F_{1\rho} + F_{2\rho} + F_{3\rho}) \,. \tag{21}$$

By explicitly implementing this cancellation, the integration over phase space is well behaved for all beam energies.

IV. RESULTS AND CONCLUSIONS

The Tables show that the coefficients of κ_4 in the cross section Eq. (3) are small which makes a value for κ_4 almost impossible to determine independent of the value of κ_3. For example Figs. 3 and 4 show the cross section for the Z process with $\sqrt{s} = 13$ and $\sqrt{s} = 100$ as a function of κ_3 for two values of κ_4. At $\sqrt{s} = 13$ TeV with

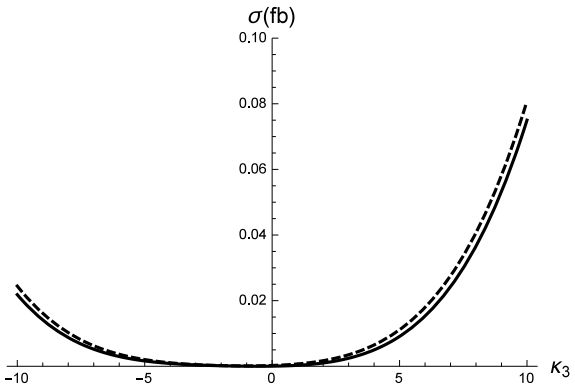

FIG. 3. The cross section for $pp \to ZHHH + X$ from $q\bar{q} \to ZHHH$ for $\sqrt{s} = 13$ TeV is shown as a function of κ_3 for $\kappa_4 = 1$ (solid line) and $\kappa_4 = 10$ (dashed line).

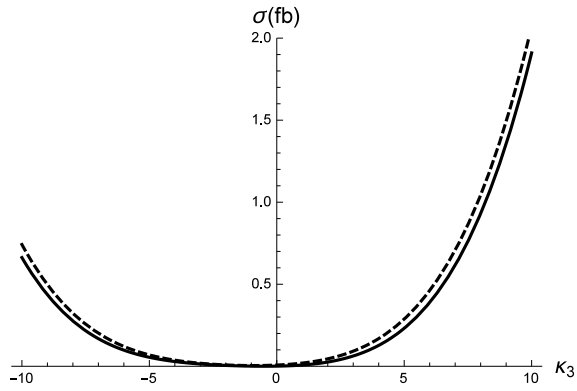

FIG. 4. The cross section for $pp \to ZHHH + X$ from $q\bar{q} \to ZHHH$ for $\sqrt{s} = 100$ TeV is shown as a function of κ_3 for $\kappa_4 = 1$ (solid line) and $\kappa_4 = 10$ (dashed line).

$\kappa_3 = 1$ the difference in the cross section between $\kappa_4 = 1$ and $\kappa_4 = 10$ is 4.2×10^{-4} fb. For $\sqrt{s} = 100$ TeV the same difference is 1.2×10^{-2} fb and if $\kappa_3 = 10$ the difference is still less than 0.16 fb. Figures 5 and 6 illustrate this further by fixing κ_3 near 1 and varying κ_4 to find that the cross sections change by only small fractions of a femtobarn. For the W^+ process the contributions that include the quartic Higgs coupling are again too small to measure κ_4 or even to determine if it is nonzero. This is illustrated in Figs. 7 and 8.

The total cross section for the W^- process is smaller than that for W^+ by a factor of 2.66, 2.24, 2.19, 1.75, 1.57, 1.47 for $\sqrt{s} = 8$, 13, 14, 33, 60, 100 TeV. The ratios of the individual cross sections (eg., σ_{44}) vary from these numbers by less than 10%.

The parameter κ_3 can be determined from processes with two Higgs bosons in the final state. For example, the subprocess $gg \to HH$ obviously depends on the three Higgs coupling as does $gg \to t\bar{t}HH$ [5–21]. Processes with three Higgs bosons in the final state are necessary to determine κ_4. We show that the processes considered here are not sufficient at any energy to even verify the existence of a four Higgs coupling. This is most obvious from Figure 2 where the coefficients of κ_4 (dashed lines) are very small compared to most of the other partial

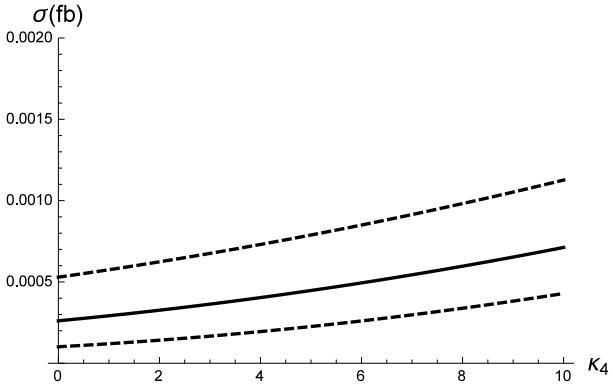

FIG. 5. The variation of the cross section for $pp \to ZHHH + X$ from $q\bar{q} \to ZHHH$ for $\sqrt{s} = 13$ TeV is shown for $\kappa_3 = 1$ (solid line) and the dashed band $0.5 \leq \kappa_3 \leq 1.5$ as a function of κ_4.

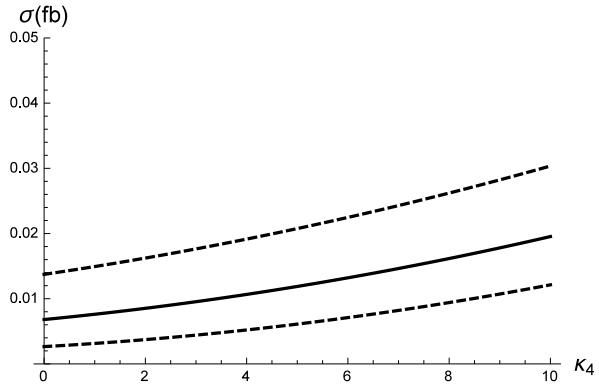

FIG. 6. The variation of the cross section for $pp \to ZHHH + X$ from $q\bar{q} \to ZHHH$ for $\sqrt{s} = 100$ TeV is shown for $\kappa_3 = 1$ (solid line) and the dashed band $0.5 \leq \kappa_3 \leq 1.5$ as a function of κ_4.

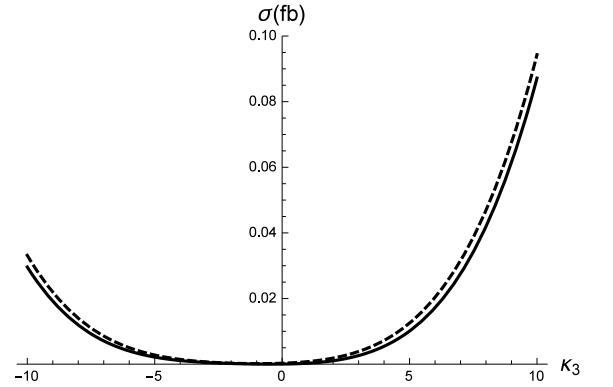

FIG. 7. The cross section for $pp \to W^+HHH + X$ from $q\bar{q} \to W^+HHH$ for $\sqrt{s} = 13$ TeV is shown as a function of κ_3 for $\kappa_4 = 1$ (solid line) and $\kappa_4 = 10$ (dashed line).

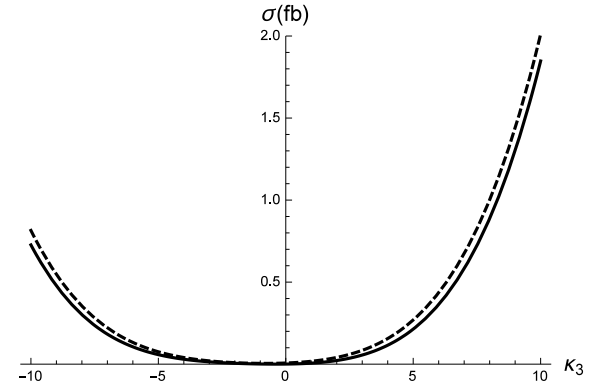

FIG. 8. The cross section for $pp \to W^+HHH + X$ from $q\bar{q} \to W^+HHH$ for $\sqrt{s} = 100$ TeV is shown as a function of κ_3 for $\kappa_4 = 1$ (solid line) and $\kappa_4 = 10$ (dashed line).

cross sections. In general the problem of determining κ_4 will be very difficult. Similar conclusions have been reached by Binoth, Karg, Kauer, and Rückl [22] and others [23, 24] for the gluon fusion process $gg \to HHH$.

Acknowledgements

D. A. D. was supported in part by the U. S. Department of Energy under Award No.DE-FG02-12ER41830, C. K. was supported in part by the U. S. Department of Energy under Award No.DE-FG02-13ER41979 and W. W. R. was supported in part by the National Science Foundation under Grant No. PHY 1068020.

[1] G. Aad *et al.* [ATLAS Collaboration], Phys. Lett. B **716**, 1 (2012) doi:10.1016/j.physletb.2012.08.020 [arXiv:1207.7214 [hep-ex]].
[2] S. Chatrchyan *et al.* [CMS Collaboration], Phys. Lett. B **716** (2012) 30 doi:10.1016/j.physletb.2012.08.021 [arXiv:1207.7235 [hep-ex]].
[3] P. Nadolsky, *et. al*, Phys. Rev. D 78, 013004 (2008).
[4] T. Han and S. Willenbrock, Phys. Lett. B **273**, 167 (1991).
[5] D. A. Dicus, C. Kao and S. S. D. Willenbrock,Phys. Lett. B **203**, 457 (1988).

[6] E. W. N. Glover and J. J. van der Bij, Nucl. Phys. B **309**, 282 (1988).
[7] S. Dawson, S. Dittmaier and M. Spira, Phys. Rev. D **58**, 115012 (1998).
[8] M. J. Dolan, C. Englert and M. Spannowsky, JHEP **1210**, 112 (2012) [arXiv:1206.5001 [hep-ph]].
[9] J. Baglio, A. Djouadi, R. Grber, M. M. Mhlleitner, J. Quevillon and M. Spira, JHEP **1304**, 151 (2013) [arXiv:1212.5581 [hep-ph]].
[10] F. Goertz, A. Papaefstathiou, L. L. Yang and J. Zurita, JHEP **1306**, 016 (2013) [arXiv:1301.3492 [hep-ph]].
[11] A. J. Barr, M. J. Dolan, C. Englert, D. E. F. de Lima and M. Spannowsky, arXiv:1412.7154 [hep-ph].
[12] A. Arhrib, R. Benbrik, C. H. Chen, R. Guedes and R. Santos, JHEP **0908**, 035 (2009) [arXiv:0906.0387 [hep-ph]].
[13] D. de Florian and J. Mazzitelli, Phys. Lett. B **724**, 306 (2013) [arXiv:1305.5206 [hep-ph]].
[14] B. Hespel, D. Lopez-Val and E. Vryonidou, JHEP **1409**, 124 (2014) [arXiv:1407.0281 [hep-ph]].
[15] N. Liu, S. Hu, B. Yang and J. Han, JHEP **1501**, 008 (2015) [arXiv:1408.4191 [hep-ph]].
[16] D. de Florian and J. Mazzitelli, Phys. Rev. Lett. **111**, 201801 (2013).
[17] R. Frederix, S. Frixione, V. Hirschi, F. Maltoni, O. Mattelaer, P. Torrielli, E. Vryonidou and M. Zaro, Phys. Lett. B **732**, 142 (2014) [arXiv:1401.7340 [hep-ph]].
[18] S. Dawson, A. Ismail and I. Low, Phys. Rev. D **91**, no. 11, 115008 (2015) [arXiv:1504.05596 [hep-ph]].
[19] D. A. Dicus, C. Kao, and W. W. Repko, Phys. Rev. D **92**, no. 9, 093003 (2015) [arXiv:1504.02334 [hep-ph]].
[20] Q. H. Cao, Y. Liu and B. Yan, arXiv:1511.03311 [hep-ph].
[21] Q. H. Cao, B. Yan, D. M. Zhang and H. Zhang, Phys. Lett. B **752**, 285 (2016) [arXiv:1508.06512 [hep-ph]].
[22] T. Binoth, S. Karg, N. Kauer and R. Rückl, Phys. Rev. D **74**, 113008 (2006) [hep-ph/0608057].
[23] A. Papaefstathiou and K. Sakurai, JHEP **1602**, 006 (2016) [arXiv:1508.06524 [hep-ph]].
[24] C. Y. Chen, Q. S. Yan, X. Zhao, Y. M. Zhong and Z. Zhao, Phys. Rev. D **93**, no. 1, 013007 (2016)[arXiv:1510.04013 [hep-ph]].

$\sqrt{s}$	σ_{44}	σ_{3333}	σ_{433}	σ_{40}	σ_{330}	σ_{43}	σ_{0}	σ_{333}	σ_{30}	σ_{33}	σ_{TOT}
8	$4.72\ 10^{-7}$	$1.20\ 10^{-6}$	$1.43\ 10^{-6}$	$2.38\ 10^{-6}$	$3.38\ 10^{-6}$	$6.03\ 10^{-6}$	$7.69\ 10^{-6}$	$9.01\ 10^{-6}$	$3.05\ 10^{-5}$	$3.60\ 10^{-5}$	$9.80\ 10^{-5}$
13	$1.57\ 10^{-6}$	$3.61\ 10^{-6}$	$4.47\ 10^{-6}$	$6.94\ 10^{-6}$	$9.31\ 10^{-6}$	$1.80\ 10^{-5}$	$2.32\ 10^{-5}$	$2.55\ 10^{-5}$	$9.05\ 10^{-5}$	$1.09\ 10^{-4}$	$2.92\ 10^{-4}$
14	$1.85\ 10^{-6}$	$4.21\ 10^{-6}$	$5.22\ 10^{-6}$	$8.01\ 10^{-6}$	$1.07\ 10^{-5}$	$2.08\ 10^{-5}$	$2.70\ 10^{-5}$	$2.94\ 10^{-5}$	$1.05\ 10^{-4}$	$1.27\ 10^{-4}$	$3.39\ 10^{-4}$
33	$9.37\ 10^{-6}$	$1.90\ 10^{-5}$	$2.46\ 10^{-5}$	$3.47\ 10^{-5}$	$4.38\ 10^{-5}$	$9.24\ 10^{-5}$	$1.23\ 10^{-4}$	$1.24\ 10^{-4}$	$4.64\ 10^{-4}$	$5.84\ 10^{-4}$	$1.52\ 10^{-3}$
60	$2.43\ 10^{-5}$	$4.67\ 10^{-5}$	$6.16\ 10^{-5}$	$8.41\ 10^{-5}$	$1.04\ 10^{-4}$	$2.26\ 10^{-4}$	$3.06\ 10^{-4}$	$2.97\ 10^{-4}$	$1.14\ 10^{-3}$	$1.45\ 10^{-3}$	$3.74\ 10^{-3}$
100	$5.15\ 10^{-5}$	$9.55\ 10^{-5}$	$1.27\ 10^{-4}$	$1.70\ 10^{-4}$	$2.07\ 10^{-4}$	$4.61\ 10^{-4}$	$6.26\ 10^{-4}$	$5.96\ 10^{-4}$	$2.31\ 10^{-3}$	$2.97\ 10^{-3}$	$7.62\ 10^{-3}$

TABLE I. Individual contributions to Eq. (3) for $pp \to ZHHH + X$. $\sqrt{s}$ is the center of mass energy in TeV. All cross sections are in femtobarns. σ_{TOT} is the sum of the contributions (the total cross section if $\kappa_3 = \kappa_4 = 1$).

$\sqrt{s}$	σ_{44}	σ_{3333}	σ_{433}	σ_{40}	σ_{330}	σ_{43}	σ_{0}	σ_{333}	σ_{30}	σ_{33}	σ_{TOT}
8	$6.58\ 10^{-7}$	$1.63\ 10^{-6}$	$1.96\ 10^{-6}$	$2.27\ 10^{-6}$	$3.17\ 10^{-6}$	$7.26\ 10^{-6}$	$6.14\ 10^{-6}$	$1.07\ 10^{-5}$	$2.87\ 10^{-5}$	$4.16\ 10^{-5}$	$1.04\ 10^{-4}$
13	$2.03\ 10^{-6}$	$4.53\ 10^{-6}$	$5.65\ 10^{-6}$	$6.00\ 10^{-6}$	$7.96\ 10^{-6}$	$1.99\ 10^{-5}$	$1.70\ 10^{-5}$	$2.78\ 10^{-5}$	$7.79\ 10^{-5}$	$1.17\ 10^{-4}$	$2.85\ 10^{-4}$
14	$2.36\ 10^{-6}$	$5.19\ 10^{-6}$	$6.52\ 10^{-6}$	$6.58\ 10^{-6}$	$9.02\ 10^{-6}$	$2.28\ 10^{-5}$	$1.96\ 10^{-5}$	$3.16\ 10^{-5}$	$8.93\ 10^{-5}$	$1.34\ 10^{-4}$	$3.27\ 10^{-4}$
33	$1.08\ 10^{-5}$	$2.12\ 10^{-5}$	$2.78\ 10^{-5}$	$2.66\ 10^{-5}$	$3.34\ 10^{-5}$	$9.15\ 10^{-5}$	$8.08\ 10^{-5}$	$1.21\ 10^{-4}$	$3.55\ 10^{-4}$	$5.54\ 10^{-4}$	$1.32\ 10^{-3}$
60	$2.66\ 10^{-5}$	$5.01\ 10^{-5}$	$6.65\ 10^{-5}$	$6.13\ 10^{-5}$	$7.56\ 10^{-5}$	$2.13\ 10^{-4}$	$1.91\ 10^{-4}$	$2.77\ 10^{-4}$	$8.29\ 10^{-4}$	$1.31\ 10^{-3}$	$3.10\ 10^{-3}$
100	$5.43\ 10^{-5}$	$9.95\ 10^{-5}$	$1.33\ 10^{-4}$	$1.20\ 10^{-4}$	$1.64\ 10^{-4}$	$4.21\ 10^{-4}$	$3.81\ 10^{-4}$	$5.40\ 10^{-4}$	$1.63\ 10^{-3}$	$2.62\ 10^{-3}$	$6.14\ 10^{-3}$

TABLE II. Same as Table I except for $pp \to W^+HHH + X$.